pp.123—134 CLIMATE, ENVIRONMENT & GEOPHYSICAL FLUID DYNAMICS 123

A NUMERICAL STUDY ON THE OROGRAPHIC EFFECT ON THE COLD SURGE IN SOUTHERN CHINA

Lee Kwok Lun

Department of Physics, The Chinese University of Hong Kong, Hong Kong

ZHANG Ming

LASG, Institute of Atmospheric Physics, Chinese Academy of Sciences, Beijing 100080, China

Abstract

A simple fine mesh limited area NWP model is designed to investigate the effect of terrain on the NE winter monsoon in Southern China. In the winter half year, cold narrow ridges are often observed along the southeast coast of China when the cold air invades southward by the eastern path. From the results of the numerical experiments, it is found that the formation of the narrow ridge is due to the blocking of cold air by Wuyi Mountain. The funnelling effect of Taiwan Strait also enhances the formation of such a ridge.

I. Introduction

During the outburst of NE winter monsoon, cold air over Siberia and Mongolia sweeps southward to continental China. Usually the cold air follows three paths to the south: the western, the middle and the eastern path. As the cold air follows the eastern path, it will first reach Inner Mongolia and Northeastern China, and then the anticyclone continues to move eastward. But the low level cold air turns southwestward, passes over the Gulf of Chihli (Bohai Sea) and Northern China, and invades the middle and lower courses of the Yangtze River (Changjiang River). Cold air of sufficient strength can pass over Nanling Mountain and invade Southern China including the Hong Kong area. On the synoptic charts, there is always observed a cold narrow ridge extending from Northern China to the Southern China along the southeast coast when the cold air is moving southward by the eastern path. The narrow ridge is also associated with a cold front at its southern rim. Activities of such a ridge have significant effect on the weather of Southern China including Hong Kong. The southward incursion of the cold ridge will bring strong NE winds, a drop in temperature and rainy weather to the area. Forecasters in the area around Southern China and Hong Kong often call such activity of cold air a "cold surge". The accuracy in predicting the motion of such a surge often decides whether the weather forecast in Southern China (including Hong Kong area) is successful or not. Both Lam (1976) and Chu (1978) showed that the surge arrivals in Hong Kong are related to bursts of the winter monsoon induced by perturbations in the mid-tropospheric zonal westerlies at middle and high latitudes and a forecast technique based on 500 hPa pattern has been developed to forecast the surge arrival. Other methods by Morrice (1973), Lai (1987) and Lau (1991) based on surface pressure pattern have also been developed for the same purpose. The prediction of strength of overnight easterly was also discussed by Chang (1989). However, the above methods are all

empirical and the formation of the narrow ridge still left unexamined. Thus, to understand the mechanism of the formation and moving pattern of such cold narrow ridge is of great importance.

Having observed many discussions of orographically trapped coastal features as documented by Gill (1977), Dorman (1985) and Holland et al. (1986), Lam and Poon of Royal Observatory Hong Kong (ROHK) believe that formation of the narrow ridge is affected by the terrain distribution in the Southern China. To prove this, a limited area numerical model incorporated with rather steep terrain is designed to investigate the southward incursion of cold air along the eastern path. Some definite conclusions emerge from this study.

II. The Numerical Model

1. Governing Equations

In deriving the governing equations, we have chosen the terrain-following σ-coordinate as the vertical coordinate to simplify the lower boundary conditions in the presence of terrain. By making the hydrostatic assumption, the governing equations can be written as

$$\frac{\partial u}{\partial t} = -M\left(u\frac{\partial u}{\partial x} + v\frac{\partial u}{\partial y}\right) - \dot{\sigma}\frac{\partial u}{\partial \sigma} - M\left(\frac{\partial \Phi}{\partial x} + H\frac{\partial P}{\partial x}\right) + f^{*}v + D_{u}, \tag{1}$$

$$\frac{\partial v}{\partial t} = -M\left(u\frac{\partial v}{\partial x} + v\frac{\partial v}{\partial y}\right) - \dot{\sigma}\frac{\partial v}{\partial \sigma} - M\left(\frac{\partial \Phi}{\partial y} + H\frac{\partial P}{\partial y}\right) - f^{*}u + D_{v}, \tag{2}$$

$$\frac{\partial H}{\partial t} = -M\left(u\frac{\partial H}{\partial x} + v\frac{\partial H}{\partial y}\right) - \dot{\sigma}\frac{\partial H}{\partial \sigma} - \kappa \cdot H \cdot \left(\frac{\dot{\sigma}}{\sigma} + \dot{P}\right) + \kappa\dot{Q} + D_{H}, \tag{3}$$

$$\frac{\partial q}{\partial t} = -M\left(u\frac{\partial q}{\partial x} + v\frac{\partial q}{\partial y}\right) - \dot{\sigma}\frac{\partial q}{\partial \sigma} + E_{1} - E_{2} + D_{q}, \tag{4}$$

$$\frac{\partial P}{\partial t} = -M^{2}\int_{0}^{1}\left[\frac{\partial}{\partial x}\left(\frac{u}{M}\right) + \frac{\partial}{\partial y}\left(\frac{v}{M}\right)\right]d\sigma - M\int_{0}^{1}\left(u\frac{\partial P}{\partial x} + v\frac{\partial P}{\partial y}\right)d\sigma, \tag{5}$$

$$\dot{\sigma} = -M^{2}\int_{0}^{\sigma}\left[\frac{\partial}{\partial x}\left(\frac{u}{M}\right) + \frac{\partial}{\partial y}\left(\frac{v}{M}\right)\right]d\sigma' - M\int_{0}^{\sigma}\left(u\frac{\partial P}{\partial x} + v\frac{\partial P}{\partial y}\right)d\sigma' - \sigma\frac{\partial P}{\partial t}, \tag{6}$$

$$\frac{\partial \Phi}{\partial \sigma} = -\frac{H}{\sigma}, \tag{7}$$

where $H = RT$, $\kappa = R / C_{p}$ in which R is the universal gas constant and C_{p} is the specific heat capacity at constant pressure, $P = \ln p_{s}$, $\dot{P} = \frac{\partial P}{\partial t} + M\left(u\frac{\partial P}{\partial x} + v\frac{\partial P}{\partial y}\right)$, E_{1} is evaporation, E_{2} is precipitation, $\dot{Q}$ is the diabatic heating rate, D's are the dissipation terms. The composite Coriolis parameter f^{*} is given by

$$f^{*} = f + M^{2}\left[v\frac{\partial}{\partial x}\left(\frac{1}{M}\right) - u\frac{\partial}{\partial y}\left(\frac{1}{M}\right)\right]$$

and all other symbols have their usual meanings.

2. Numerical Methods

For simplicity the grid interval in both horizontal and vertical directions are regular. The

horizontal interval d and vertical interval $\triangle\sigma$ are both adjustable. The field variables are all defined on the same grid points. Generally two configurations were used in the numerical experiments. In the first configuration, the horizontal dimension of the model domain is 59×59 with 10 vertical levels, i.e. $\triangle\sigma = 0.1$ and $d \approx 0.5^\circ$ (about 50 km). The mesh is rather fine in this configuration. In the other configuration we take 30×30 to be the horizontal dimension with 5 vertical intervals, i.e. $\triangle\sigma = 0.2$ and $d \approx 1^\circ$ (about 100 km) and the resolution is smaller than the first one. The domain of the limited area model is 10—39°N and 105—134°E and is the same in the two configurations. Fig. 1 shows the model domain and the distribution of grid points. In the followings, the results of the numerical experiments are all based on the first configuration unless otherwise stated.

The second order centered difference scheme is chosen for spatial differencing, and forward–iterative backward scheme is used for time integration. The time step for integration is 2.5 minutes for the fine grid configuration and is double for the coarse grid one.

3. Boundary Conditions

Since the model is mainly used to perform numerical experiments, time varying lateral boundary condition is used. Boundary values of field variables from analysis are read in every 1.5 or 3 hours (however, only 6–hour analysis is available from ROHK, the unavailable one is obtained by linear interpolation). Relaxation is added to the outermost four rings to reduce the imbalance between the newly read boundary values and the original fields. It can be done by adding a relaxation term on the right sides of the prognostic equations. Eqs. (1)—(4) in the boundary zone is written in the following form

$$\frac{\partial F}{\partial t} = A(F) - K(F - \tilde{F}), \tag{8}$$

where K is the relaxation coefficient which decreases nonlinearly from the boundary and $\tilde{F}$ is the boundary value from the analysis. Apart from relaxation, the boundary effects are also reduced by increasing the value of horizontal dissipation coefficient. In some experiments investigating the effect of changing the interval of renewing the boundary values, the results of forecast

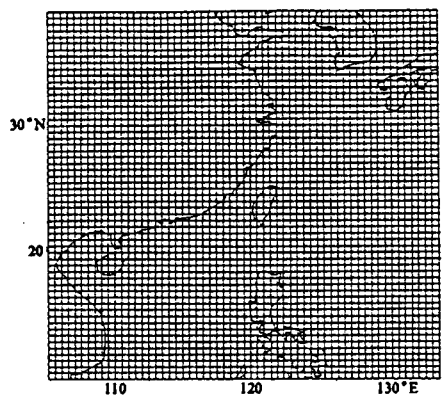

Fig. 1. The horizontal domain and distribution of grid points of the limited area model.

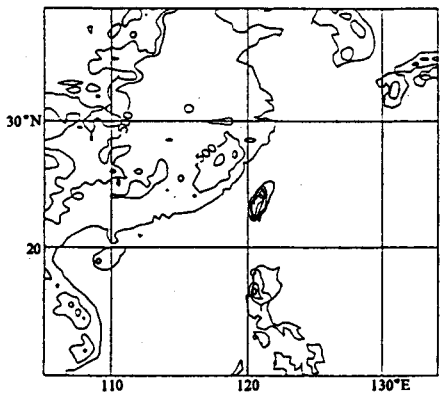

Fig. 2. The whole terrain field (in 500 m vertical interval) in the model.

were found to be nearly the same if the boundary values are renewed in 1. 5 or 3 hour intervals, with the former a little bit better. However, if the boundary values are renewed 6-hour, the result is quite poor, but still better than that from fixed boundary condition. In the numerical experiments reported in this paper, the boundary values are renewed 6-hourly.

Action of drag, sensible heat flux and evaporation are considered at the lower boundary and will be explained later. For simplicity, the upper boundary condition is taken to be $\partial F / \partial\sigma|_{\sigma=0} = 0$, where F is one of the 3-D field variables.

4. Physical Processes

(1) *The Treatment of Terrain*

Actual terrain field is used in the model. The highest point in the model domain is about 2000 m as shown in Fig. 2. Owing to the existence of rather steep terrain in the model, Corby's (1972) scheme is used to calculate the pressure gradient force and the finite difference scheme is as follows:

$$-\frac{\partial\Phi}{\partial x} - H\frac{\partial P}{\partial x} \approx -\overline{\delta_x\Phi}^x - \overline{\overline{H}^x\delta_x P}^x, \tag{9}$$

$$-\frac{\partial\Phi}{\partial y} - H\frac{\partial P}{\partial y} \approx -\overline{\delta_y\Phi}^y - \overline{\overline{H}^y\delta_y P}^y, \tag{10}$$

where

$$\overline{F}^x = \frac{1}{2}\left[F\left(i+\frac{1}{2}\right)+F\left(i-\frac{1}{2}\right)\right] \quad \text{and} \quad \delta_x F = \frac{1}{\Delta x}\left[F\left(i+\frac{1}{2}\right)-F\left(i-\frac{1}{2}\right)\right]$$

The geopotential is calculated by the following scheme:

$$\Phi_N = \Phi_s - H_N \ln\sigma_N \ , \tag{11}$$

$$\Phi_k = \Phi_{k+1} - \frac{1}{2}(H_k + H_{k+1})(\ln\sigma_k - \ln\sigma_{k+1}), \quad k = 1,2,\cdots,N \tag{12}$$

where N is the code of the lowest level, $\Phi_s = gz_s$ with z_s being the height of terrain. The finite difference form of the terms $H\partial P / \partial x$ and $H\partial P / \partial y$ in the thermodynamic Eq.(3) are also written as

$$\overline{\overline{H}^x\delta_x P}^x \qquad \text{and} \qquad \overline{\overline{H}^y\delta_y P}^y$$

for consistency in the whole model. After adopting such scheme, the model performs well in the presence of terrain.

(2) *Physical Processes in the Boundary Layer*

For simplicity, the physical processes in the boundary layer are evaluated by bulk aerodynamics. In the lowest level of the model (i.e. the Nth level), the action of drag, sensible heat flux and evaporation are parameterized as

$$K_\sigma\frac{\partial^2 u}{\partial\sigma^2} \approx -\frac{CC_D}{h}\sqrt{u_N^2+v_N^2}\cdot u_N - K_\sigma\frac{u_N - u_{N-1}}{h^2}, \tag{13}$$

$$K_\sigma\frac{\partial^2 v}{\partial\sigma^2} \approx -\frac{CC_D}{h}\sqrt{u_N^2+v_N^2}\cdot v_N - K_\sigma\frac{v_N - v_{N-1}}{h^2}, \tag{14}$$

$$K_\sigma \frac{\partial^2 H}{\partial \sigma^2} \approx -\frac{CC_D}{h}\sqrt{u_N^2 + v_N^2} \cdot (H_w - H_s) - K_\sigma \frac{H_N - H_{N-1}}{h^2}, \tag{15}$$

$$K_\sigma \frac{\partial^2 q}{\partial \sigma^2} \approx -\frac{CC_D}{h}\sqrt{u_N^2 + v_N^2} \cdot (q_{ss} - q_s) - K_\sigma \frac{q_N - q_{N-1}}{h^2}$$

$$= E_1 - K_\sigma \frac{q_N - q_{N-1}}{h^2}, \tag{16}$$

where C_D is the drag coefficient and C is a constant proportional to K_σ and is taken to be 1.25 $\times 10^{-4}$ m^{-1}, $H_w = RT_w$ and $H_s = RT_s$ with T_w and T_s being the temperature of the underlying surface (i.e. sea surface or land surface) and the air temperature just above the underlying surface, q_{ss} and q_s are the saturated specific humidity and specific humidity just above the underlying surface. The values of T_s and q_s are interpolated from T_N and q_N respectively.

(3) *Evaluation of Diabatic Heating*

Diabatic heating in the model includes only the release of latent heat by the large scale rain and cumulus convective rain. The large scale rain is evaluated by the most common iterative scheme and the cumulus convective rain is calculated by the modified Kuo' s (1975) parameterization of cumulus convection.

III. Experimental Results and Discussions

By the simple model developed, four events of southward incursion of cold air from the eastern path are chosen for numerical experiments. The initial fields used in the case studies are given in Table 1. Only case I will be described in detail while the other three will be briefly mentioned.

Table 1. The local standard time (LST) and date of the initial fields used in the case studies

Case study	Date and time of initial field
I	20 LST 24 February 1991
II	14 LST 4 January 1992
III	02 LST 18 February 1992
IV	14 LST 20 March 1992

The synoptic charts of the first case study are shown in Fig. 3. All the charts are shown at 18 GMT (02 LST at 120°E). Initially the center of high pressure is located around Tianjin. It continues to move eastward and finally reaches the southern sea of Korean Peninsula on 26 February. We can see that there is a narrow ridge extending from the center of high pressure to the Southern China along the southeast coast and is very obvious on 25 February. Figs. 4 and 5 show the time sequences of streamlines (solid arrows) and isotherms (dash lines) charts of the first case study on the 1000 hPa pressure surface which are constructed from the 6-hour analysis with one degree resolution obtained from ROHK. From the streamline charts it is observed that the center of anticyclone matches the center of high pressure as shown in Fig. 3. The center of anticyclone moved eastward and finally reaches the southern sea of Korean Peninsula. As the cold air sweep southward, the streamlines along the southeast coast of China and Taiwan Strait

become closely packed. This reveals the existence of a cold surge and its effect on the southern coast of China. The characteristics of the cold surge is clearly indicated by Fig. 5(e). In the chart there is a zone of divergence around Wuyi Mountain and Nanling Mountain area. The streamlines west of Taiwan show a cyclonic curvature. Furthermore, the coastal area of Guangdong and Fujian is affected by a NE current

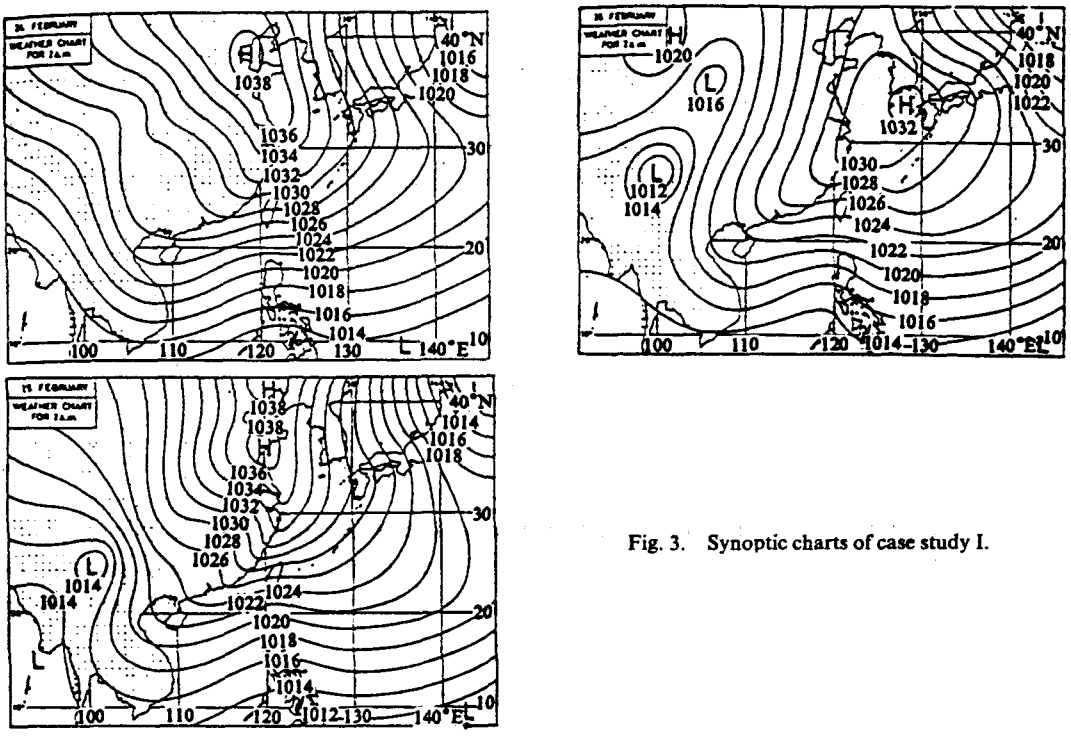

Fig. 3. Synoptic charts of case study I.

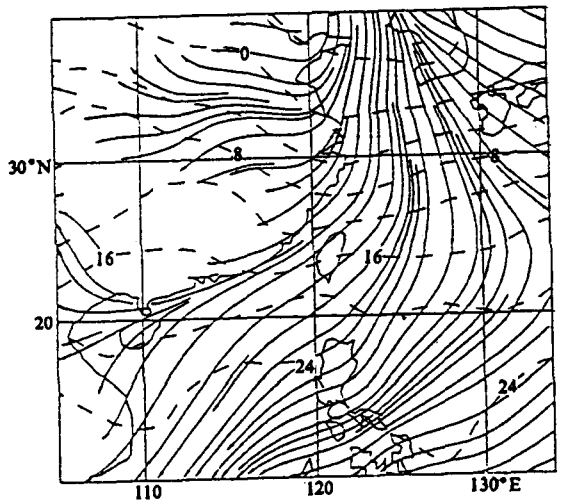

Fig. 4. 1000 hPa streamlines (solid lines) and isotherms (dash lines) from analysis. It is the initial field of case study I.

Results of the numerical experiment are presented as follows. The analysis at 20 LST, 24 February 1991 (corresponding to Fig. 4) is chosen to be the initial field of the experiment. The forecast data is output 6-hour for easy comparison with the analysis and only data on the 950 hPa pressure surface will be presented. There are two reasons in presenting the charts on the 950 hPa surface. The first reason is that the object of the research (the activities of the cold narrow ridge) is mainly a low level phenomenon. The second one is that the lowest level of the model is $\sigma = 0.95$ and the error in interpolating the physical quantities on the 950 hPa surface will be the smallest. The result of a numerical experiment by using the actual terrain is given by Fig. 6. For the 36-hour forecast (Fig. 6(f)) the center of anticyclone moves to the southwestern sea of Korean Peninsula. The track is approximately the same as the actual case but the speed of movement is a little bit slower (compare with the position of the center of anticyclone in Fig. 5(f)). Such lowering in speed of the movement of the weather system is probably due to the use of finite different approximation in the numerical model. In the 6-hour forecast (Fig. 6(a)), the streamlines in the southeast coastal area become closely packed, showing that the cold surge is formed. The same observation is also made in the analysis (Fig. 5(a)). In the 30-hour forecast,

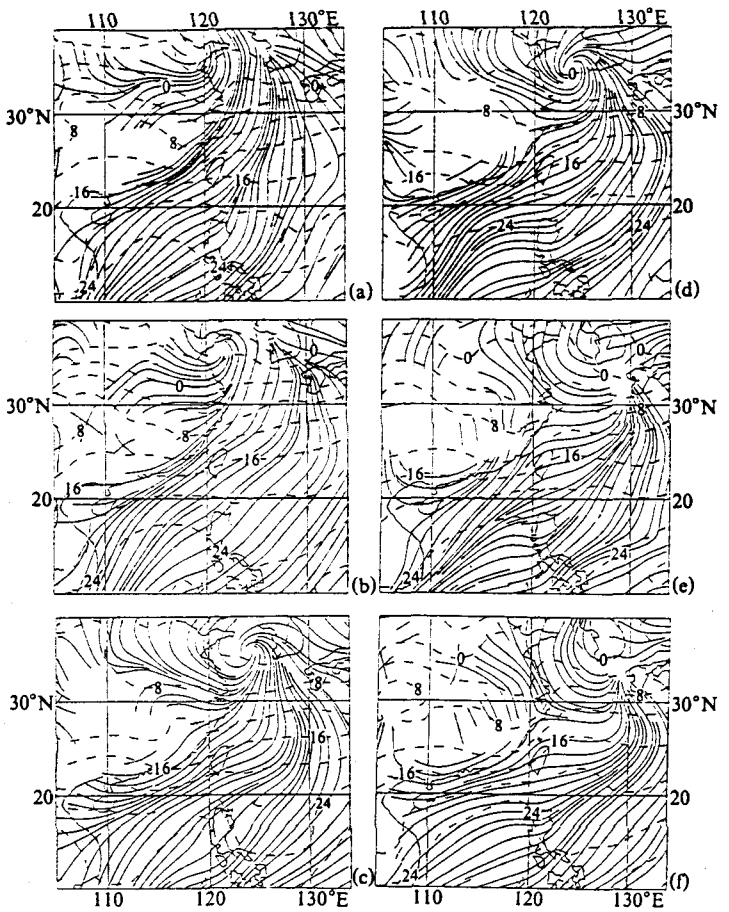

Fig. 5. 6-hour time sequences of analysis on 1000 hPa after 0h (Fig.4). (a) 6h; (b) 12h; (c) 18h; (d) 24h; (e) 30h; (f) 36h.

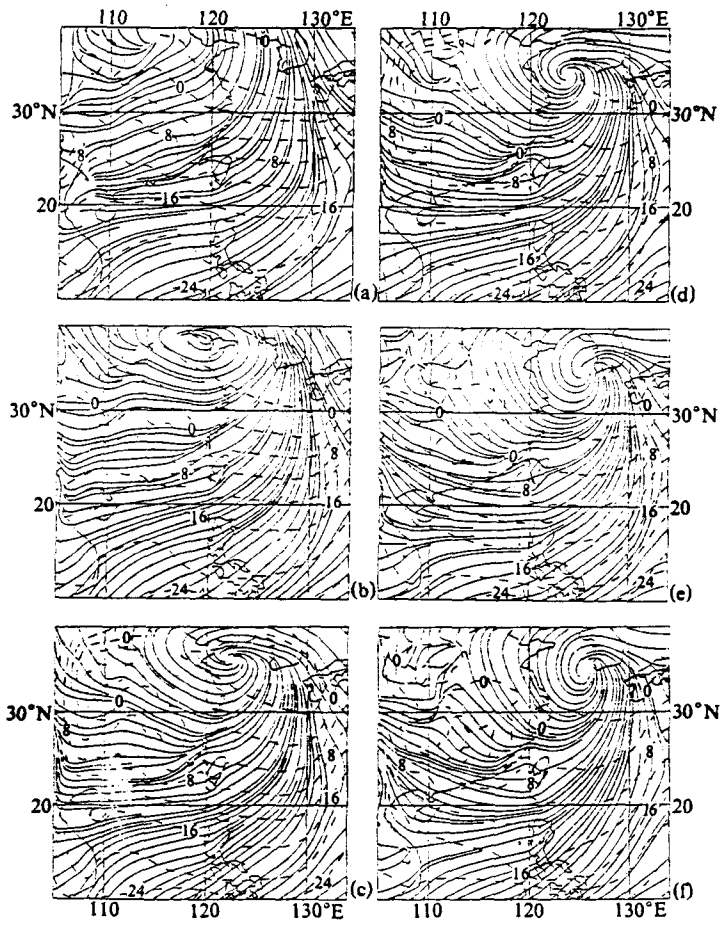

Fig. 6. 6-hour time sequence of forecast on 950 hPa with whole terrain field after 0h (Fig.4). (a) 6h; (b) 12h; (c) 18h; (d) 24h; (e) 30h; (f) 36h.

the cold narrow ridge along the southeast coastal area is clearly revealed by the streamline chart (Fig 6(e)). The divergence zone around Wuyi and Nanling Mountains is clearly shown on the chart. The cyclonic curvature of the streamlines west of Taiwan and the northeast current along the coast of Guangdong and Fujian is also forecast (compare Fig.5(e) with Fig.6(e)). From the 36-hour forecast (Fig.6(f)), the above characteristics are more obvious and they are also found in the analysis (Fig. 5(f)).

The wind fields of simulation and analysis are very similar when comparing Fig.5 with Fig.6, showing that the result of simulation is quite satisfactory. However, the values in the temperature fields in the two figures should not be compared directly because they are on different pressure surfaces. Nevertheless, a cold tongue protruding southward along the southeast coast is observed in the simulation result (Fig. 6). Similar observation is made in Fig. 5 but the strength of the cold tongue is weaker.

A simulation with the whole terrain field removed is performed to investigate the effect of the terrain. The 30-hour forecast streamline and temperature fields are shown in Fig. 7(a) with the same initial field as the above experiment. The center of the anticyclone is moving at the

same track as in the previous simulation. However, the characteristics of cold narrow ridge are not observed. The streamlines are very smooth and no zone of divergence around Wuyi and Nanling Mountains is observed. Furthermore, neither the cyclonic curvature of streamlines west of Taiwan nor the protruded cold tongue appear. Comparing Fig.6 with Fig.7, obviously the characteristics stated above are closely related to the existence of terrain.

To further explore the influences of terrain on the formation of the cold narrow ridge, three more numerical experiments are performed using the same initial field as in the previous experiments. The terrain in the southeast coastal area is removed in the first experiment. To be precise, a straight line is drawn from Leizhou Peninsula to the delta of Yangtze River and all the terrain east to the line is removed, preserving the terrain of Taiwan Island only. In the second experiment the terrain east of the above straight line with height higher than 500 m is lowered to 500 m and the terrain of Taiwan is removed. In the third experiment the original terrain is multiplied by a factor of 1.2. The results of the first two experiments are demonstrated in Fig. 7(b) and Fig. 7(c) respectively.

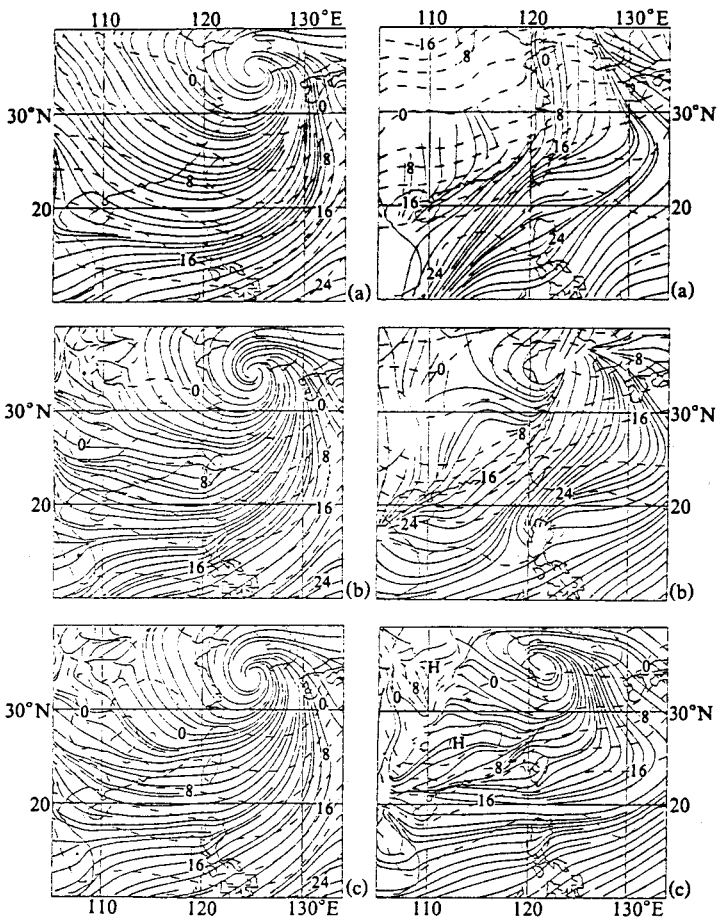

Fig. 7. 30-hour forecast of case study I with (a) no terrain; (b) coastal terrain removed; (c) Taiwan removed and coastal terrain lowered.

Fig. 8. Case study II. (a) Initial field (analysis); (b) 30-hour analysis after (a); (c) 30-hour forecast.

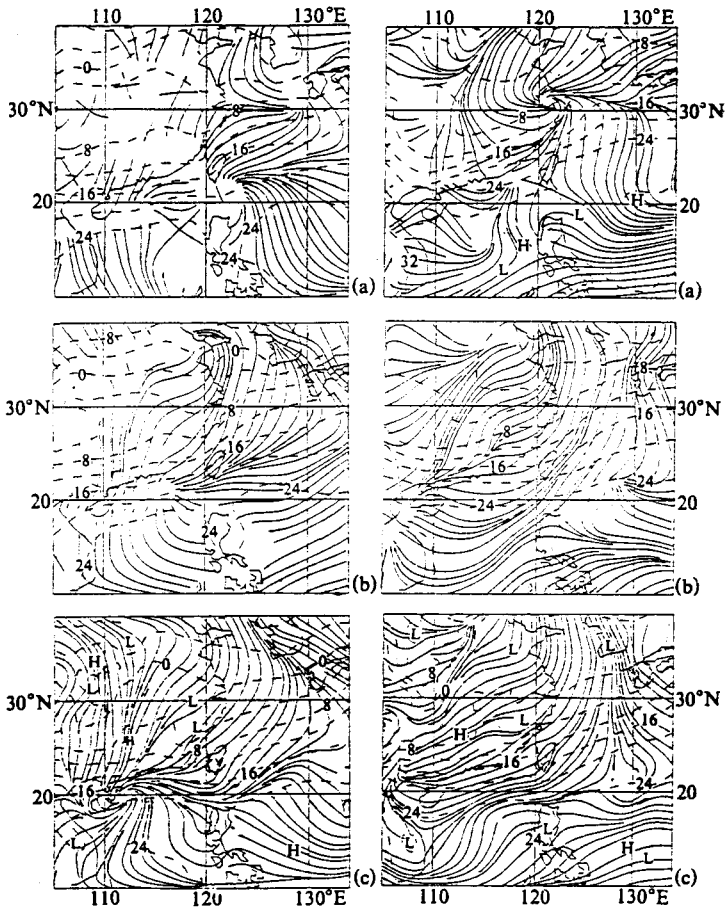

Fig. 9. Case study III. (a) initial field (analysis); (b) 30-hour analysis after (a); (c) 30-hour forecast.

Fig. 10. Case study IV. (a) initial field (analysis); (b) 30-hour analysis after (a); (c) 30-hour forecast.

From Fig. 7(b), the characteristics of the cold narrow ridge do not appear. The zone of divergence around Wuyi Mountain is not obvious and the cold tongue around the southeastern coast disappears. However, the cyclonic curvature of the streamlines still exists to the west of Taiwan Island, but it is weaker compared with that one obtained from experiment with the whole terrain field. From such observations, it can be argued that the formation of the cold narrow ridge is mainly determined by the existence of the terrain in the southeast coastal area. Furthermore, the formation of cyclonic curvature west of Taiwan is forced by the terrain of the island when the easterly passes it. Although the terrain in the southeast coastal area is lowered in the numerical experiment shown in Fig. 7(c), the existence of the characteristics of cold narrow ridge is still obvious. However, the strength it is weaker than the case when the actual terrain field is used. The cold tongue is also clearly observed in the temperature field in the experiment. It should be noted that the cyclonic curvature of streamlines west of Taiwan disappears as the terrain of the island is removed in this run. This experiment further confirms the above arguments are correct. As the height of the terrain is increased in the last experiment, the strength

of the characteristics in the wind and temperature fields become more obvious (not shown). It shows no doubt that the above characteristics are really terrain induced features.

The results of the other three case studies are shown in Fig. 8, Fig. 9 and Fig. 10 respectively. Similar results as the first case study are obtained. For simplicity, only the initial field, the 30-hour forecast with the whole terrain field used and the corresponding analysis are shown. From the 30-hour forecast, the characteristics discussed above are all shown. The streamlines along the southeastern coast become closely packed. A zone of divergence around Wuyi Mountain and Nanling Mountain area appears. The cyclonic curvature of streamlines west of Taiwan and the cold tongue are also observed. However, the closely packed streamlines, zone of divergence and cold tongue all disappear as the terrain in the southeast coastal area is removed (not shown).

IV. Explanations

In observing the results from the numerical experiment, some explanations for the formation of the characteristics are made. In general, when the cold air invades southward along the eastern path, its strength is usually weaker. Moreover, the cold air is thin and the slope of the frontal surface is not very steep. Although Wuyi Mountain is not very high, it is still enough to block the original track of the thin layer of cold air. Then the cold air pass around the mountain and so a zone of divergence is observed in the region. From the previous experiments, we can observed that the cold tongue is formed whenever the terrain of Wuyi Mountain is present, showing that the formation of such a tongue is due to the existence of the range. As the cold air from the northeast or east reaches Wuyi Mountain, it is blocked by the southeast slope of the range and wind is forced to blow parallel to the range. Thus northeasterly is the prevailing wind in the southeastern coastal area in winter monsoon. Since the cold air is trapped to move along the southeast coast, a protruded cold tongue is observed in the temperature field. Furthermore, it also reveals the existence of a narrow coastal ridge in synoptic charts. Taiwan Island is small, but it is so high that the layer of cold air passes mainly around it rather than over it. A cyclonic curvature is formed naturally in the northern branch as the cold air bends around it. In the presence of Wuyi Mountain, Taiwan Strait acts as a bottle neck and the funnelling effect causes the air to accelerate in the strait and it further enhances the cyclonic curvature. Such acceleration of cold air also facilitates the formation of the protruded cold tongue.

It should be pointed out that the characteristics in the wind and temperature fields are more obvious in the forecast results than the analysis (compare Fig.5 with Fig.6). The main reason is that the mesh of the limited area model is finer than that of analysis and the above characteristics will be smoothed out when the resolution is not high enough. The difference in pressure surface of the two figures may also be another reason.

V. Conclusions

From the results of numerical experiments in this paper, we can draw the following conclusions.

(1) In winter half year, cold narrow ridge is often observed along the Southeast China as the cold air invades southward by the eastern path. The formation of a narrow ridge is mainly due to the blocking of Wuyi Mountain. The funnelling effect of Taiwan Strait also enhances the formation of the ridge.

(2) Due to the high terrain of Taiwan Island, cold current from the east or northeast passes mainly around it rather than over it. The northern branch of the current forms a cyclonic curvature on the west of the island. The acceleration of air in the strait helps to increase the cyclonic curvature of the current.

(3) The blocking effect of Wuyi Mountain causes the thin layer of cold current to pass around it and so a zone of divergence is formed around the area.

It should be further pointed out that the model used in conducting the numerical experiments demonstrated in this paper is dry and without sensible heat flux added. By using such a simple dynamical framework, the results of simulation are rather satisfactory.

Some experiments on the resolution of numerical model are also performed by using the two configurations of the model mentioned before. For the coarse configuration ($30 \times 30 \times 5$), the characteristics in the wind and temperature fields are not clearly observed (not shown) due to low resolution. Thus, to the extent possible, increasing the resolution of numerical model will facilitate the improvement of result from numerical forecast and simulation.

Acknowledgments We wish to thank Prof. K. Young of The Chinese University of Hong Kong for his discussion. We also wish to thank Mr. Poon Hoi To and Mr. Lam Chiu Ying of Royal Observatory Hong Kong for their valuable opinions and data provided.

References

Chang K. M. (1989), Prediction of the strength of overnight easterly winds in Hong Kong in winter, *Royal Observatory Technical Note*, **No.79**.

Chu E. W. K. (1978), A method for forecasting the arrival of cold surge in Hong Kong, *Royal Observatory Technical Note*, **No.43**.

Corby G. A. et al. (1972), A general circulation model of the atmosphere suitable for long period integrations, *Quart. J. R. Met. Soc.*, **98:** 809—832.

Dorman C. E. (1985), Evidence of Kelvin waves in California's marine layer and related eddy generation, *Mon. Wea. Rev.*, **113:** 827—839.

Gill A. E. (1977), Coastally trapped waves in the atmosphere, *Quart. J. R. Met. Soc.*, **103:** 431—440.

Holland G. J. and Leslie L. M. (1986), Ducted coastal ridging over SE Australia, *Quart. J. R. Met. Soc.*, **112:** 731—748.

Lai S. T. (1989), Short range forecasting of northerly surge, *Royal Observatory Technical Note*, **No. 83.**

Lam C. Y. (1976), 500 hPa trough passing over Lake Baikal and the arrival of surge at Hong Kong, *Royal Observatory Forecaster's Note*, **No.1**.

Lau S. Y. (1991), Movement of troughs and cold fronts over South China in the late cold season, *Royal Observatory Technical Note* (local), **No.56**.

Peng Li and Kuo H. L. (1975), A numerical simulation of the development of tropical cyclones, *Tellus*, **27:** No.2, 133—144.

Morrice A. M. (1973), Quantitative forecasting of winter monsoon in Hong Kong, *Royal Observatory Technical Note*, **No.35**.